Supplementary Information

Autophagy deficiency leads to protection from obesity and insulin resistance by inducing Fgf21 as a 'mitokine'

Kook Hwan Kim, Yeon Taek Jeong, Hyunhee Oh, Seong Hun Kim, Jae Min Cho, Yo-Na Kim, Su Sung Kim, Do Hoon Kim, Kyu Yeon Hur, Hyoung Kyu Kim, TaeHee Ko, Jin Han, Hong Lim Kim, Jin Kim, Sung Hoon Back, Masaaki Komatsu, Hsiuchen Chen, David C. Chan, Morichika Konishi, Nobuyuki Itoh, Cheol Soo Choi & Myung-Shik Lee

<CONTENTS>

Nature Medicine doi:10.1038/nm.3014

SUPPLEMENTARY RESULTS

Increased Fgf21 in mice fed leucine-deficient diet

To evaluate the role of mitochondrial stress-Atf4-Fgf21 axis in more physiologically relevant models, we challenged mice with calorie-restricted (35% reduction of calorie intake) diet as a nutrient restriction model or leucine-deficient diet as a nutrient deficiency model. Body and fat weights were significantly reduced in both leucine-deficient diet-fed and calorie-restricted diet-fed C57BL/6 mice compared to respective control diet-fed C57BL/6 mice, which was accompanied by enhanced glucose tolerance (**Supplementary Fig. 11a–c** and data not shown). Notably, serum FGF21 concentration was increased in mice fed leucine-deficient diet compared to mice fed control diet (**Supplementary Fig. 11d**). However, we did not observe change of Fgf21 concentration in mice fed calorie-restricted diet (data not shown), in contrast to a recent paper showing a mild increase of Fgf21 after calorie-restricted diet[1]. Differences in experimental procedures (50% vs. 35% reduction of calorie intake) might explain discrepant results. In addition, we found increased *Fgf21* mRNA expression and Atf4 activation in the liver of mice fed leucine-deficient diet compared to mice fed control diet, consistent with a recent paper[2], while such changes were absent in skeletal muscle (**Supplementary Fig. 11e**), suggesting that the activation of hepatic Atf4-Fgf21 axis contributes to the increased serum Fgf21 concentration in mice fed leucine-deficient diet. However, the expression of Fgf21 and Atf4 was not changed in the liver and skeletal muscle of mice fed calorie-restricted diet compared to mice fed control diet (data not shown). Furthermore, mtOxPhos gene expression was downregulated in the liver of mice fed leucine-deficient diet compared to mice fed control diet (**Supplementary Fig. 11f**). Notably, the rate of *ex vivo* β-oxidation was increased in WAT and BAT of mice fed leucine-

deficient diet compared to mice fed control diet (**Supplementary Fig. 11g**), although the difference in WAT was marginal (P = 0.056). However, there were no differences in the rate of β-oxidation in skeletal muscle and liver between the two groups (data not shown). *Ucp1* gene expression in WAT and BAT was also upregulated in mice fed leucine-deficient diet compared to mice fed control diet (data not shown). Thus, these results suggest that increased Fgf21 enhances β-oxidation and thermogenesis, leading to reduced fat mass and enhanced glucose tolerance in mice fed leucine-deficient diet. To prove this possibility, we challenged $Fgf21^{-/-}$ mice with leucine-deficient diet. In $Fgf21^{-/-}$ mice fed leucine-deficient diet, body or fat weight loss and enhanced glucose tolerance were remarkably less pronounced compared to $Fgf21^{+/+}$ mice fed leucine-deficient diet (**Supplementary Fig. 11h–j**), suggesting that increased Fgf21 partially contributes to the changes of metabolic profile in mice fed leucine-deficient diet. In contrast, there were no differences in the loss of body and fat weights, and glucose tolerance between $Fgf21^{-/-}$ and $Fgf21^{+/+}$ mice fed calorie-restricted diet (data not shown). Although it was recently reported that mice fed leucine-deficient diet exhibit reduced fat mass and increased energy expenditure[3], molecular mechanisms underlying these phenotypes have been unclear. Therefore, our data suggest that activation of Atf4-Fgf21 axis contributes to reduced fat mass and increased energy expenditure in nutrient deficiency by enhancing β-oxidation and thermogenesis.

SUPPLEMENTARY FIGURES

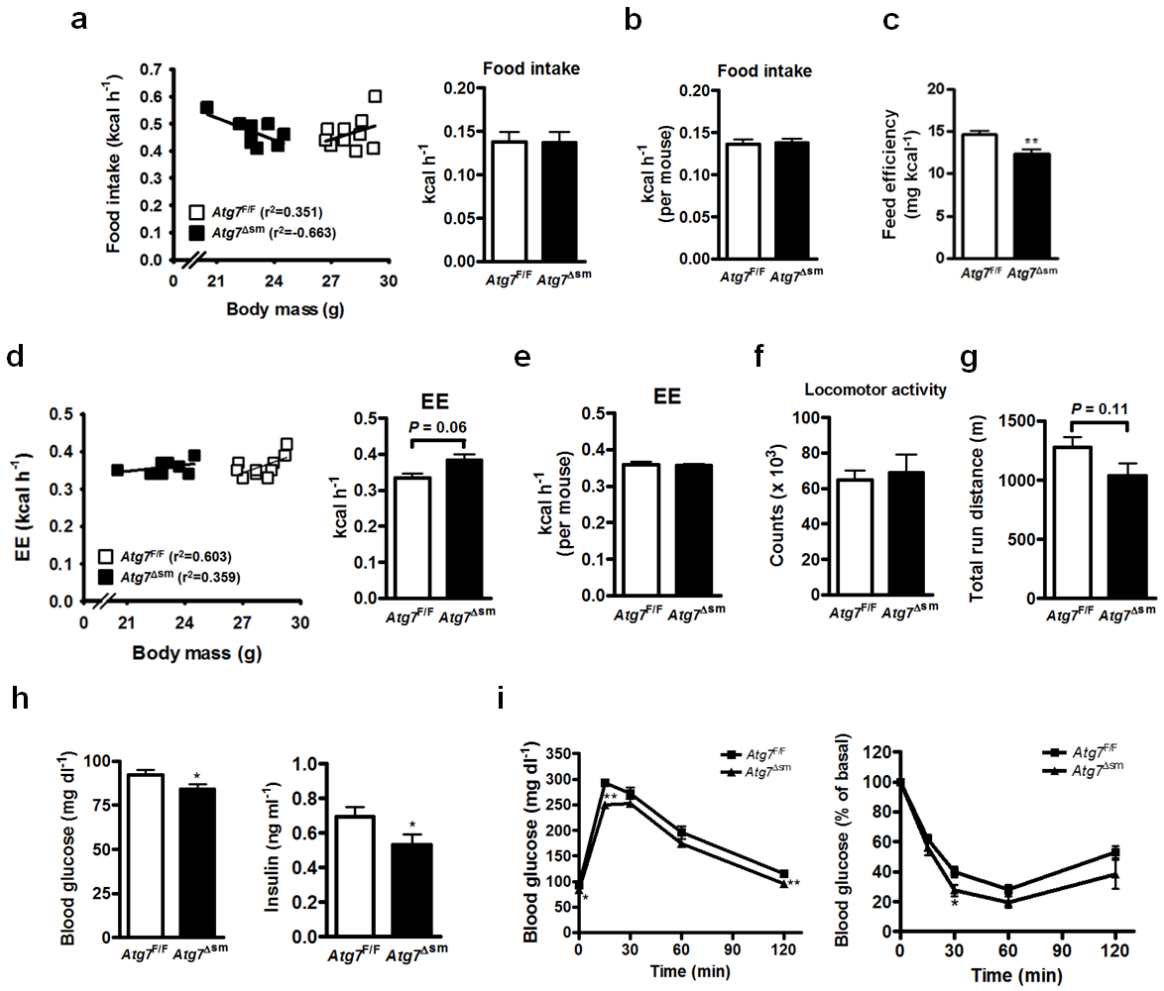

Figure S1. Enhanced glucose tolerance in *Atg7*$^{\Delta sm}$ mice fed chow diet. (**a**) Food intake plotted against body mass with fitted lines of linear regression (left) and food intake adjusted for body mass by ANCOVA (right) in 20-week-old male mice (n = 9–10). Food intake was measured during the period of indirect calorimetry. (**b**) Unadjusted food intake in 20-week-old male mice (n = 9–10). (**c**) Feed efficiency (gain of body weight per cumulated food intake) of male mice between 4 and 16 weeks of age (n = 11–14). (**d**) Energy expenditure (EE) plotted against body mass with fitted lines of linear regression (left) and EE adjusted for body mass by ANCOVA (right) in 20-week-old male mice (n = 9–10). (**e**) Unadjusted EE in 20-week-old male mice (n = 9–10). (**f**) Locomotor activity of 20-week-old male mice (n = 9–10). (**g**) Total run distance of treadmill-exercised 24-week-old mice (n = 6). (**h**) Fasting glucose (left) (n = 9) and insulin concentrations (right) (n = 14) in 20-week-old male mice fed chow. (**i**) GTT (left) and ITT (right) in 16-week-old male mice fed chow (n = 9). Data are mean ± SEM. *P < 0.05, **P < 0.01.

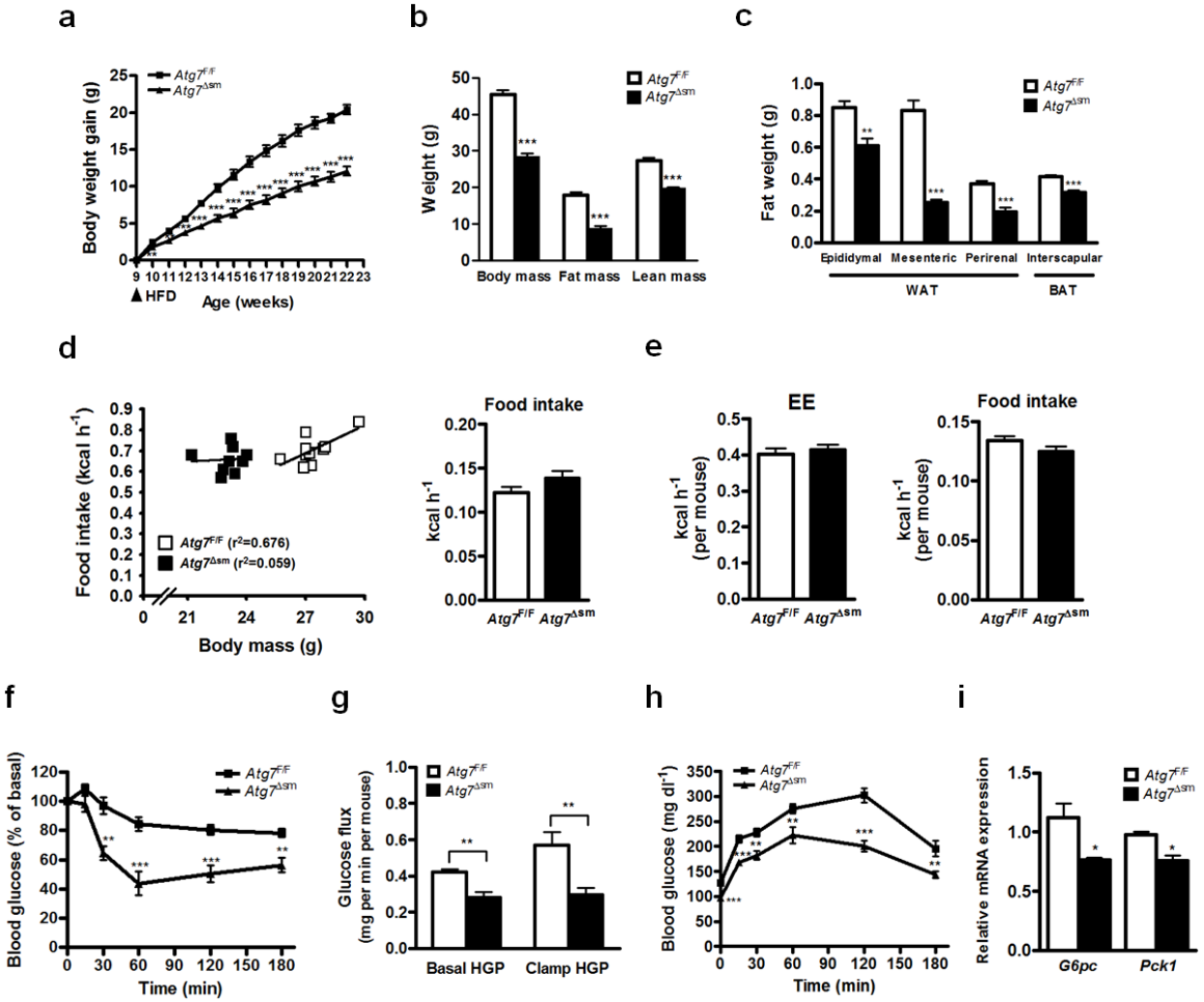

Figure S2. Decreased gain of body weight and improved insulin sensitivity in *Atg7*$^{\Delta sm}$ mice fed HFD. (**a**) Gain of body weight in male *Atg7*$^{F/F}$ and *Atg7*$^{\Delta sm}$ mice fed HFD (n = 16–23). (**b**) Body mass and composition of 24-week-old male mice fed HFD for 13 weeks (n = 8–10). (**c**) Weights of epididymal, mesenteric and perirenal WAT and interscapular brown adipose tissue (BAT) from HFD-fed mice (n = 6). (**d**) Food intake plotted against body mass with fitted lines of linear regression (left) and food intake adjusted for body mass by ANCOVA (right) in male *Atg7*$^{F/F}$ and *Atg7*$^{\Delta sm}$ mice fed a short-term HFD for 1 week (n = 9–10). (**e**) Unadjusted EE and food intake of HFD-fed male mice (n = 9–10). (**f**) ITT in *Atg7*$^{F/F}$ and *Atg7*$^{\Delta sm}$ mice fed HFD for 13 weeks (n = 7–10). (**g**) Hepatic glucose production (HGP) in HFD-fed mice during hyperinsulinemic-euglycemic clamp (n = 7–8). (**h**) Pyruvate tolerance test (PTT) in mice fed HFD for 13 weeks (n = 10–12). (**i**) Relative mRNA level of gluconeogenesis-associated genes in the liver of HFD-fed mice (n = 4). Data are mean ± SEM. *P < 0.05, **P < 0.01, ***P < 0.001.

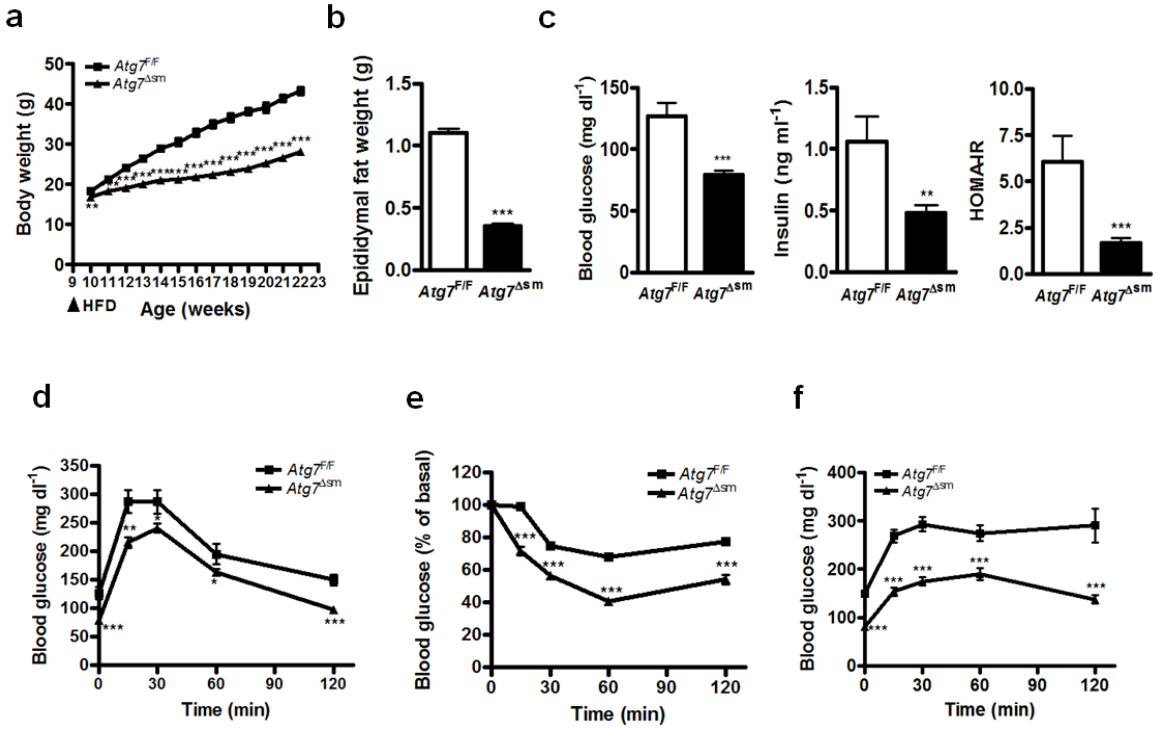

Figure S3. Reduced body weight and improved glucose profile in female *Atg7*$^{\Delta sm}$ mice fed HFD. (**a**) Body weight of female *Atg7*$^{F/F}$ and *Atg7*$^{\Delta sm}$ mice fed HFD (n = 12–18). (**b**) Weight of epididymal fat from HFD-fed female mice (n = 6). (**c**) Fasting glucose and insulin concentrations, and HOMA-IR index in female mice fed HFD (n = 6–13). (**d**–**f**) GTT (n = 6–13) (**d**), ITT (n = 9–17) (**e**), and PTT (n = 7–15) (**f**) in female mice fed HFD. Data are mean ± SEM. *P < 0.05, **P < 0.01, ***P < 0.001.

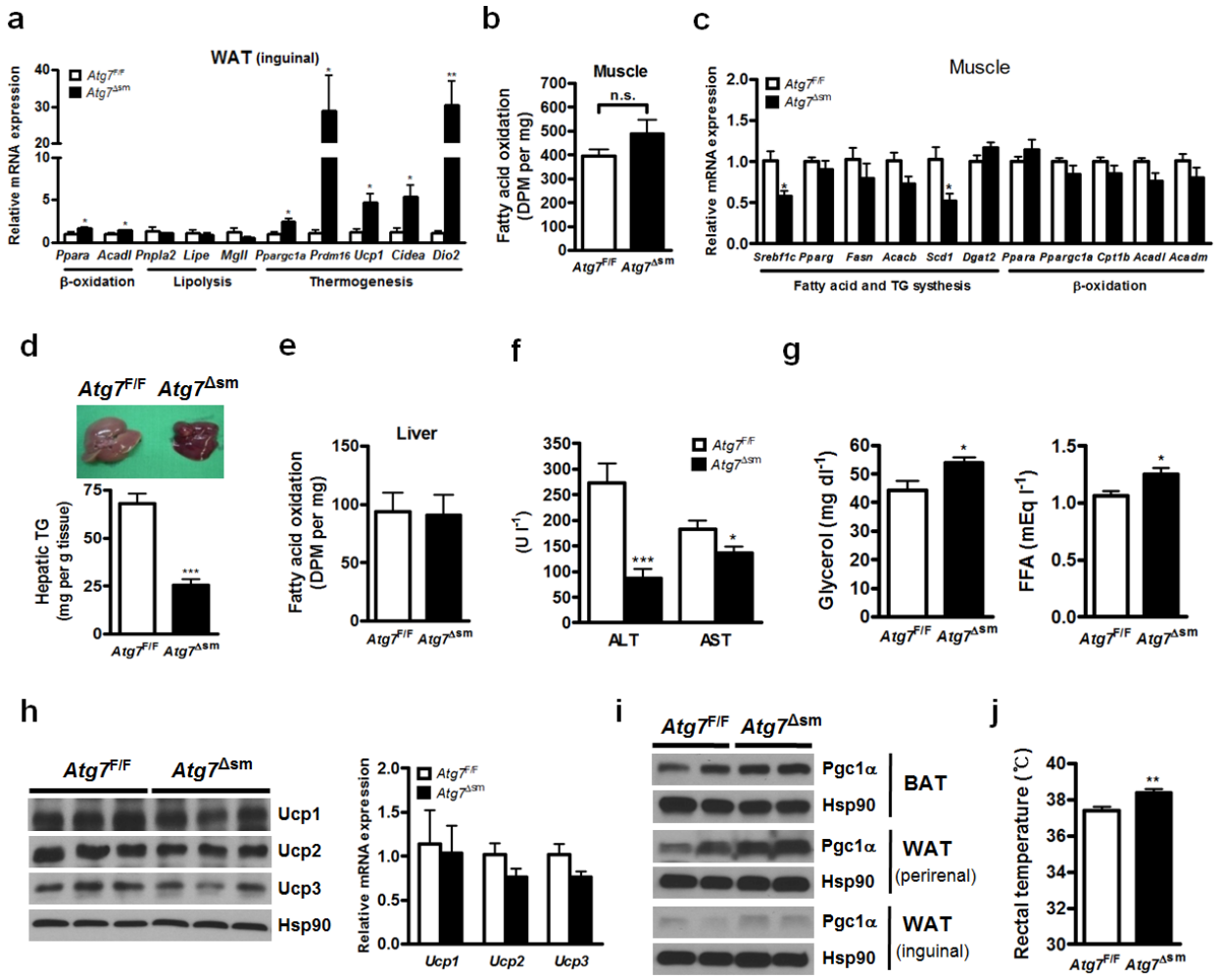

Figure S4. Improved metabolic profile in *Atg7*$^{\Delta sm}$ mice. (**a**) Relative expression of genes of β-oxidation, lipolysis and thermogenesis in inguinal WAT of HFD-fed mice (n = 3). (**b**) *Ex vivo* β-oxidation in extensor digitorum longus muscle of mice fed HFD (n = 6–8). (**c**) Relative expression of genes of fatty acid and triacylglycerol (TG) synthesis or β-oxidation in GAS muscle of HFD-fed mice (n = 3). (**d**) Gross image (upper) and TG content (lower) of the liver from mice fed HFD (n = 6–9). (**e**) *Ex vivo* β-oxidation in the liver of mice fed HFD (n = 5–7). (**f**) Serum ALT and AST concentrations in male mice fed HFD for 13 weeks (n = 12–15). (**g**) Serum glycerol (n = 7) and FFA concentrations (n = 9–12) in fasted mice on HFD. (**h**) Ucp protein (left) and mRNA levels (right) in GAS muscle of mice fed HFD (n = 3). (**i**) Immunoblotting for Pgc1α in WAT (perirenal and inguinal) and BAT of mice fed HFD. (**j**) Rectal temperature in mice fed HFD for 8 weeks (n = 8–9). Data are mean ± SEM. *P < 0.05, **P < 0.01, ***P < 0.001. (n.s. indicates not significant).

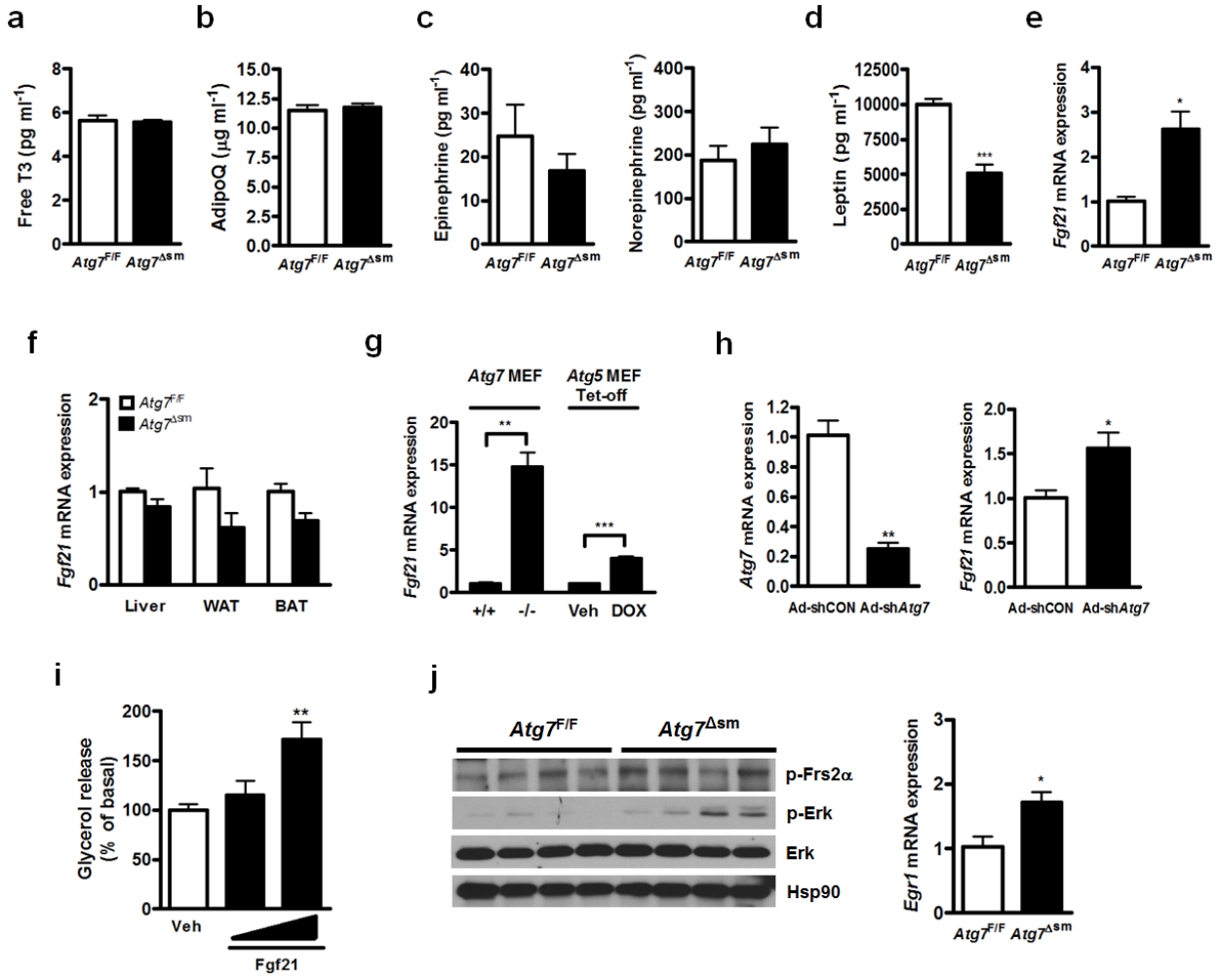

Figure S5. Increased Fgf21 expression in *Atg7*$^{\Delta sm}$ mice and autophagy-deficient cells. (**a**–**d**) Serum free T3 (**a**) (n = 4), adipoQ (**b**) (n = 10–11), plasma epinephrine or norepinephrine (**c**) (n = 5), and leptin concentrations (**d**) (n = 10–12) in *Atg7*$^{F/F}$ and *Atg7*$^{\Delta sm}$ mice fed HFD for 13 weeks. (**e**) Relative *Fgf21* mRNA expression in SOL muscle of mice fed chow (n = 3). (**f**) Relative *Fgf21* mRNA expression in the liver, WAT and BAT of *Atg7*$^{F/F}$ and *Atg7*$^{\Delta sm}$ mice fed chow (n = 3). (**g**) Relative *Fgf21* mRNA expression in *Atg7*-null and Tet-off *Atg5*-null MEFs cultured with or without doxycycline (Dox; 50 ng ml^{-1}) for 30 days. (**h**) Relative *Atg7* and *Fgf21* mRNA expression in C2C12 myotubes infected with adenovirus expressing shCON or sh*Atg7* for 72 h. (**i**) Lipolytic effect of Fgf21 on WAT *ex vivo*. Glycerol release was measured after treatment of epididymal fat from C57BL/6 mice with vehicle (Veh) or recombinant Fgf21 (0.2 and 1 μg ml^{-1}) for 3 h. Assay was performed in triplicate. (**j**) Immunoblotting for p-Frs2α, p-Erk, Erk and Hsp90 in the liver of *Atg7*$^{F/F}$ and *Atg7*$^{\Delta sm}$ mice fed HFD (left). Relative *Egr1* mRNA expression in the liver of mice fed HFD (n = 3) (right). Data are mean ± SEM. *P < 0.05, **P < 0.01 ***P < 0.001.

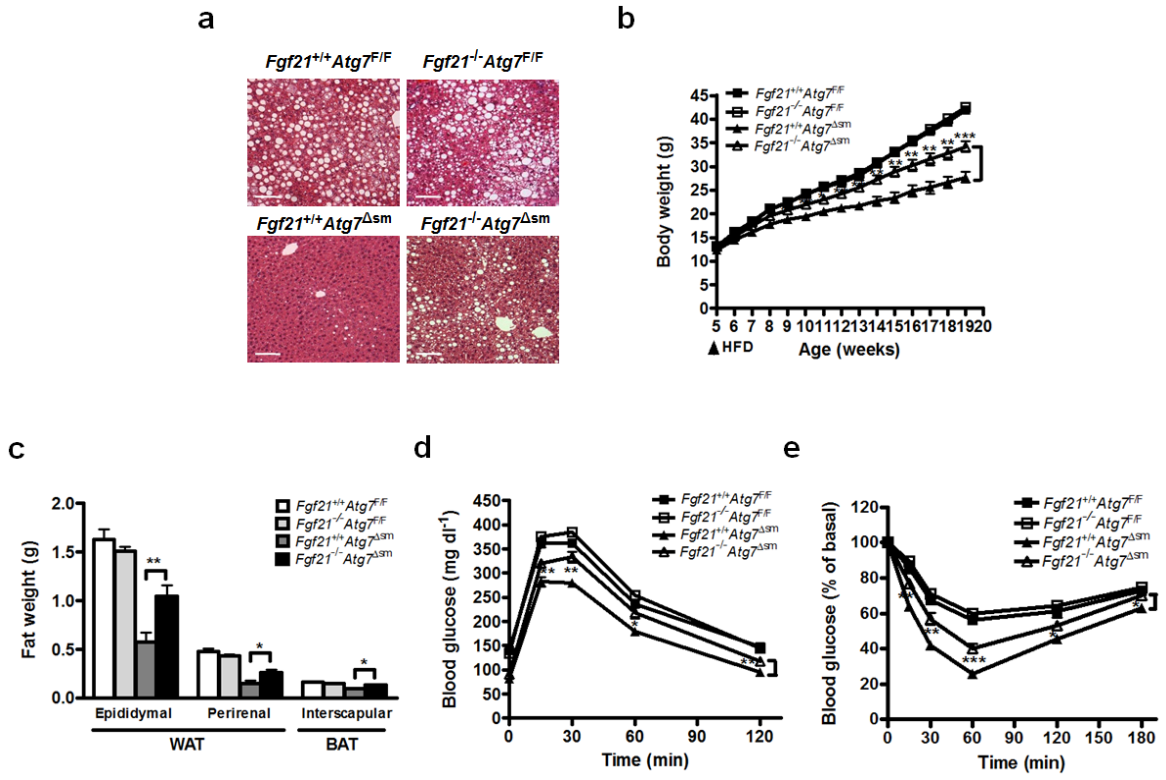

Figure S6. The role of Fgf21 in improved metabolic profiles of *Atg7*$^{\Delta sm}$ mice fed HFD. (**a**) H&E staining of the liver from male *Fgf21*$^{+/+}$*Atg7*$^{F/F}$, *Fgf21*$^{-/-}$*Atg7*$^{F/F}$, *Fgf21*$^{+/+}$*Atg7*$^{\Delta sm}$ and *Fgf21*$^{-/-}$*Atg7*$^{\Delta sm}$ mice fed HFD for 12 weeks. (**b**–**e**) Body weight (**b**), fat weight (**c**), GTT (**d**) and ITT (**e**) in female *Fgf21*$^{+/+}$*Atg7*$^{F/F}$, *Fgf21*$^{-/-}$*Atg7*$^{F/F}$, *Fgf21*$^{+/+}$*Atg7*$^{\Delta sm}$ and *Fgf21*$^{-/-}$*Atg7*$^{\Delta sm}$ mice fed HFD for 14 weeks (n = 7–11). Data are mean ± SEM. *P < 0.05, **P < 0.01 ***P < 0.001.

Nature Medicine doi:10.1038/nm.3014

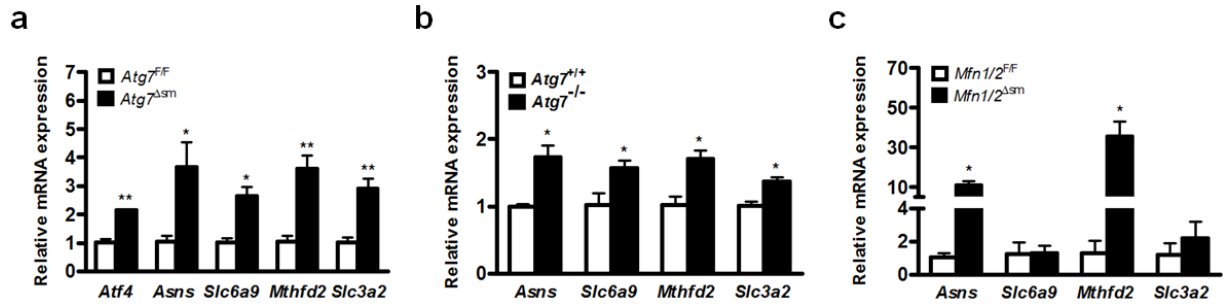

Figure S7. The expression of *Atf4* and Atf4 target genes in muscle of *Atg7*$^{\Delta sm}$ and *Mfn1/2*$^{\Delta sm}$ mice or *Atg7*-null MEFs. (**a**) Relative mRNA expression of *Atf4*, *asparagine synthetase* (*Asns*), *solute carrier family 6, member 9* (*Slc6a9*), *methylenetetrahydrofolate dehydrogenase 2* (*Mthfd2*) and *solute carrier family 3, member 2* (*Slc3a2*) in GAS muscle of male *Atg7*$^{F/F}$ and *Atg7*$^{\Delta sm}$ mice (n = 3). (**b**) Relative mRNA expression of *Asns*, *Slc6a9*, *Mthfd2* and *Slc3a2* in wild-type and *Atg7*-null MEFs. Assay was performed in triplicate. (**c**) Relative mRNA expression of Atf4 target genes in skeletal muscle of *Mfn1/2*$^{\Delta sm}$ mice. The expression of *Asns* and *Mthfd2* genes was increased in skeletal muscle of *Mfn1/2*$^{\Delta sm}$ mice. Data are mean ± SEM. **P* < 0.05, ***P* < 0.01.

Nature Medicine doi:10.1038/nm.3014

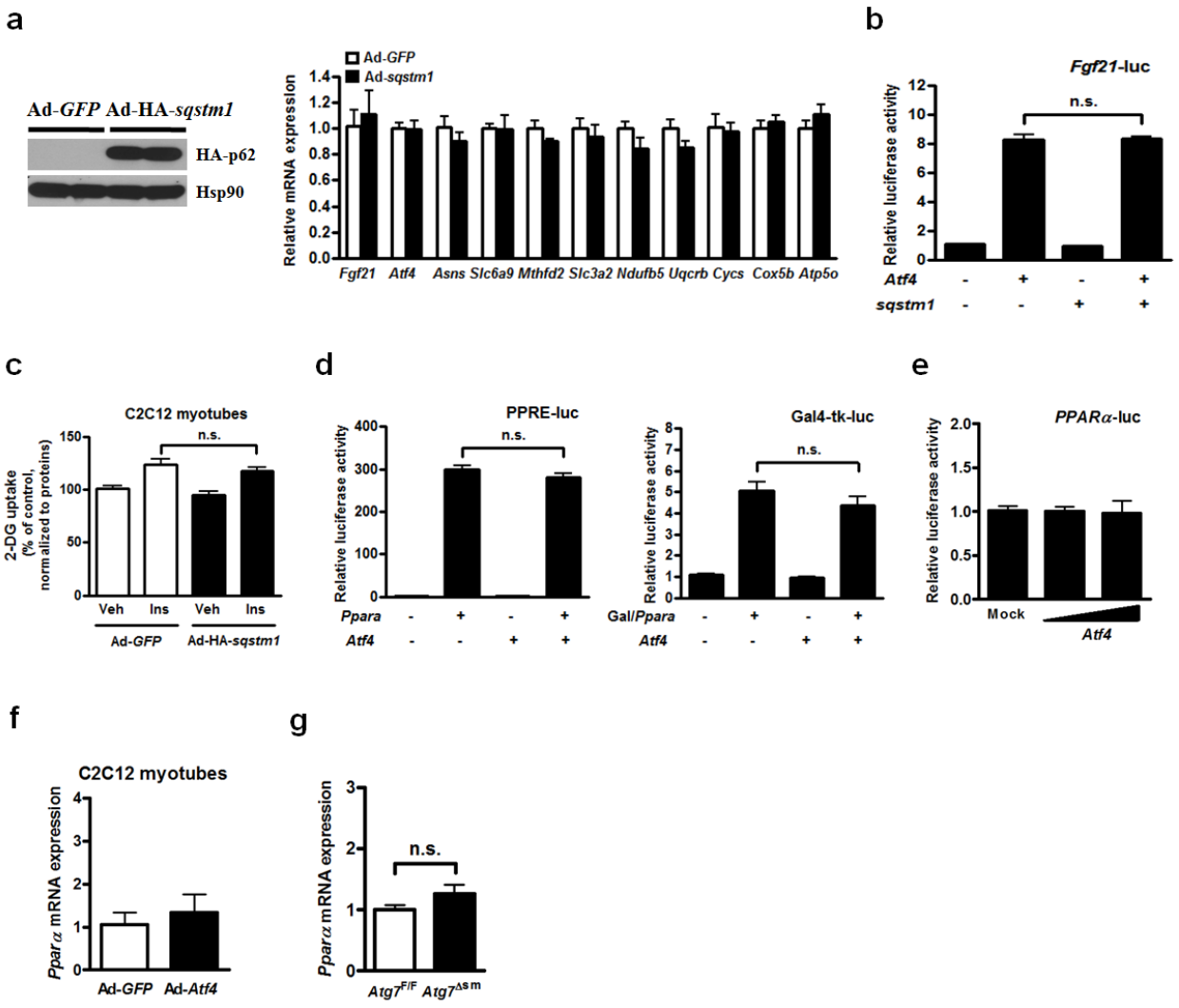

Figure S8. The role of p62 or Pparα in *Fgf21* induction by autophagy deficiency. (**a**) Immunoblotting for HA-p62 (left) and relative mRNA expression (right) in C2C12 myotubes infected with adenovirus expressing GFP or HA-*sqstm1* for 48 h. (**b**) Luciferase activity of *Fgf21* promoter in HEK293 transfected with *Atf4* with or without *sqstm1* expression vector for 24 h. (**c**) 2-DG uptake in C2C12 myotubes infected with adenovirus expressing GFP or HA-*sqstm1* for 48 h with or without insulin (Ins) treatment. (**d**) Reporter activity of PPAR response element (PPRE)-luc (left) and Gal4-tk-luc (right) in HEK293 transfected with *Ppara* (left) and Gal/*Ppara* (right) vectors, respectively, along with *Atf4* plasmid for 24 h. (**e**) Luciferase activity of *Pparα* promoter in HEK293 transfected with *Atf4* vector for 24 h. (**f**) Relative *Pparα* mRNA expression in C2C12 myotubes infected with adenovirus expressing GFP or *Atf4* for 36 h. (**g**) Relative mRNA expression of *Pparα* in GAS muscle of male $Atg7^{F/F}$ and $Atg7^{\Delta sm}$ mice (n = 3). Data are mean ± SEM (n.s. indicates not significant).

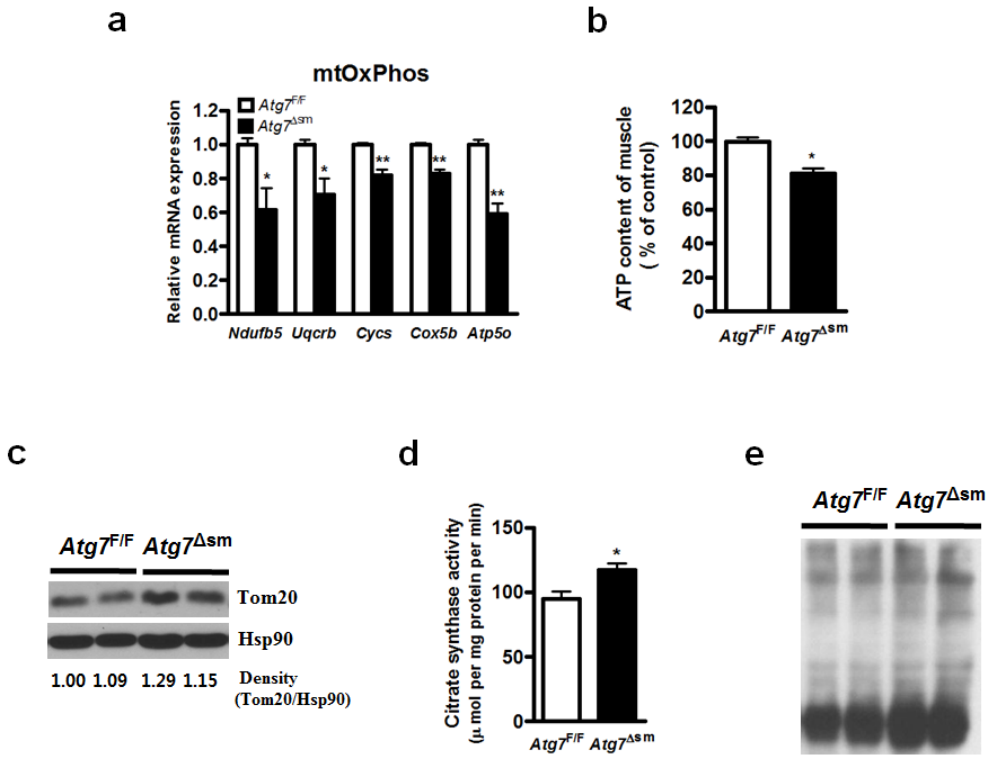

Figure S9. Impaired mtOxPhos gene expression, increased mitochondrial mass and oxidative stress in muscle of *Atg7*$^{\Delta sm}$ mice. (**a**) Relative mRNA expression of mtOxPhos genes in GAS muscle of male *Atg7*$^{F/F}$ and *Atg7*$^{\Delta sm}$ mice (n = 3). (**b**) ATP content in GAS muscle of *Atg7*$^{F/F}$ and *Atg7*$^{\Delta sm}$ mice (n = 5). (**c**) Immunoblotting for Tom20 in GAS muscle of *Atg7*$^{F/F}$ and *Atg7*$^{\Delta sm}$ mice. Relative band density was quantified using an ImageJ software. (**d**) Citrate synthase activity in GAS muscle of *Atg7*$^{F/F}$ and *Atg7*$^{\Delta sm}$ mice (n = 6–8). (**e**) Immunoblotting for carbonylated protein in GAS muscle of *Atg7*$^{F/F}$ and *Atg7*$^{\Delta sm}$ mice. Data are mean ± SEM. *P < 0.05, **P < 0.01.

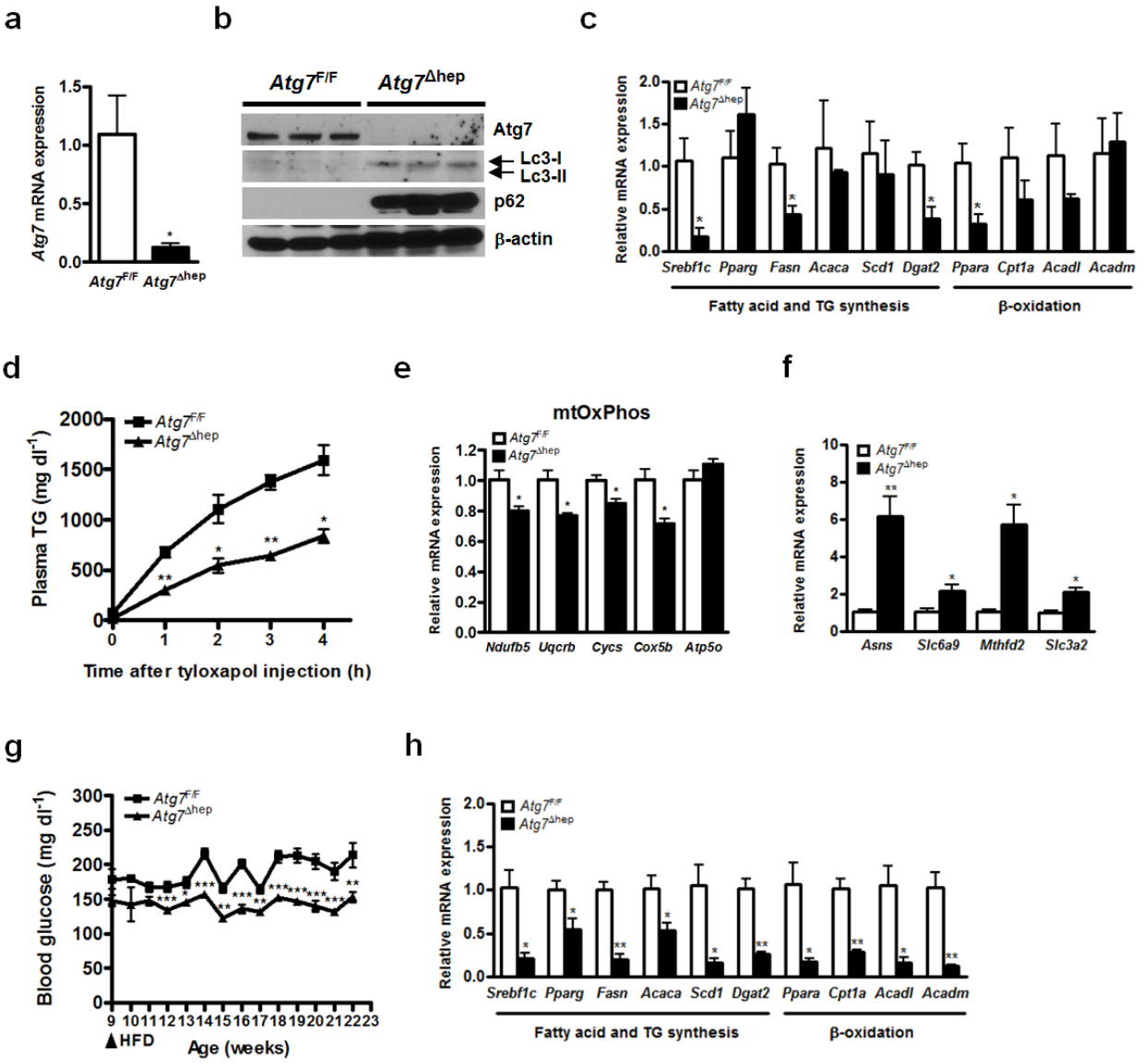

Figure S10. The changes of glucose or lipid metabolism and mtOxPhos in *Atg7*$^{\Delta hep}$ mice. (**a**,**b**) Generation of liver-specific *Atg7*-null (*Atg7*$^{\Delta hep}$) mice. Relative *Atg7* mRNA expression (**a**) and protein levels of Atg7, Lc3 and p62 (**b**) in the liver of *Atg7*$^{\Delta hep}$ mice (n = 3). (**c**) Relative mRNA expression of genes associated with fatty acid and triacylglycerol (TG) synthesis or β-oxidation in the liver of *Atg7*$^{\Delta hep}$ mice fed chow (n = 3). (**d**) Plasma TG concentration of *Atg7*$^{F/F}$ and *Atg7*$^{\Delta hep}$ mice after tyloxapol administration (n = 3). (**e**,**f**) Relative mRNA expression of mtOxPhos in primary hepatocytes (**e**) and Atf4 target genes in the liver (**f**) from *Atg7*$^{F/F}$ and *Atg7*$^{\Delta hep}$ mice fed chow (n = 3). (**g**) Nonfasting glucose concentration in *Atg7*$^{F/F}$ and *Atg7*$^{\Delta hep}$ mice fed HFD between 9 and 22 weeks of age (n = 5–7). (**h**) Relative mRNA expression of genes associated with fatty acid and TG synthesis or β-oxidation in the liver of *Atg7*$^{\Delta hep}$ mice fed HFD (n = 3). Data are mean ± SEM. *P < 0.05, **P < 0.01, **P < 0.001.

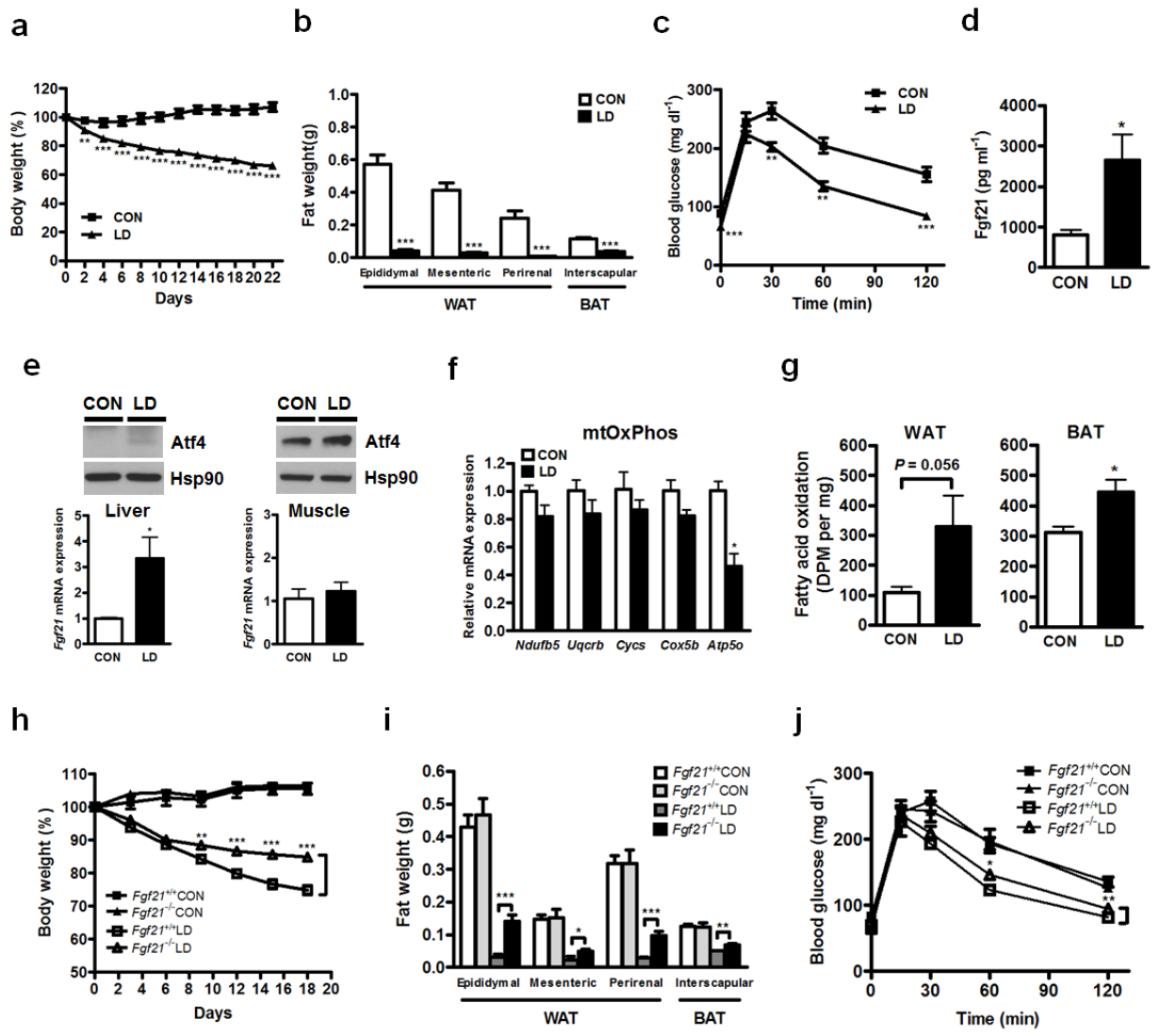

Figure S11. The role of Fgf21 in leucine-deficient (LD) diet-induced metabolic changes. (**a**) Body weight of male C57BL/6 mice fed control or LD diet between 12 and 15 weeks of age (n = 7–8). Mice on control diet were pair-fed since food intake was decreased by LD diet. (**b**–**d**) Fat weight (n = 6) (**b**), GTT (n = 7–8) (**c**) and serum Fgf21 concentration (n = 6–7) (**d**) in male C57BL/6 mice fed control or LD diet for 3 weeks. (**e**) Relative *Fgf21* mRNA expression (n = 3–4) and Atf4 protein level in the liver (left) and GAS muscle (right) of C57BL/6 mice fed control or LD diet for 3 weeks. (**f**) Relative mRNA expression of mtOxPhos genes in the liver of C57BL/6 mice fed LD diet for 3 weeks (n = 3). (**g**) *Ex vivo* β-oxidation in WAT and BAT of C57BL/6 mice fed control or LD diet for 10 days (n = 8–10). (**h**) Body weight in male $Fgf21^{+/+}$ and $Fgf21^{-/-}$ mice fed control or LD diet between 12 and 15 weeks of age (n = 5–9). (**i**,**j**) Fat weight (**i**) and GTT (**j**) in male $Fgf21^{+/+}$ and $Fgf21^{-/-}$ mice fed control or LD diet for 3 weeks (n = 5–9). Data are mean ± SEM. *P < 0.05, **P < 0.01 ***P < 0.001.

SUPPLEMENTARY METHODS

Body composition and analysis of energy balance. Fat and lean body masses were measured by a ^{1}H minispec system (LF90II; Bruker Optik) in mice fed chow or HFD. Activity, food consumption, oxygen consumption, and energy expenditure were assessed in a metabolic monitoring system (CLAMS: Columbus Instruments) for 4 days (2 days of acclimation followed by 2 days of measurement) employing 20- or 24-week-old mice fed chow diet or HFD as previously described[4]. Locomotor activity was measured by counting the number of infrared beam breaks on x- and z-axes during the measurement period. Rectal temperature was measured using a Testo 925 electronic rectal thermometer (Testo).

Hyperinsulinemic-euglycemic clamp. Seven days prior to the hyperinsulinemic-euglycemic clamp studies, indwelling catheters were placed into the right internal jugular vein. After overnight fast, [3-^{3}H]-glucose (HPLC purified; PerkinElmer) was infused at a rate of 0.05 μCi per min for 2 h to assess the basal glucose turnover. Following the basal period, hyperinsulinemic-euglycemic clamp was conducted for 140 min with a primed/continuous infusion of human insulin (126 pmol per kg during priming, 18 pmol per kg per min during infusion) (Eli Lilly), while plasma glucose was maintained at a basal concentration (~6.7 mM) as described[4]. Throughout the clamps, [3-^{3}H]-glucose was infused at a rate of 0.1 μCi per min to estimate insulin-stimulated whole-body glucose flux, and 2-deoxy-D-[1-^{14}C]-glucose (2-[^{14}C]-DG; PerkinElmer) was injected as a bolus at the 85th minute of the clamp to estimate the rate of insulin-stimulated tissue glucose uptake. Blood samples (10 μl) were taken at the end of the

basal period and during the last 45 min of the clamp for the measurement of plasma ^{3}H and ^{14}C activities.

***Glucose flux calculation*:** To determine plasma ^{3}H and ^{14}C activities, plasma was deproteinized with $ZnSO_4$ and $Ba(OH)_2$, dried to remove $^{3}H_2O$, resuspended in water and counted in scintillation fluid (Ultima gold, PerkinElmer) using a Beckman scintillation counter. The rates of basal and insulin-stimulated whole-body glucose flux were determined as the ratio of the [3-^{3}H]-glucose infusion rate (disintegrations per minute [DPM]) to the specific activity of plasma glucose (DPM per mg) at the end of the basal period and during the final 30 min of the clamp experiment, respectively. Hepatic glucose production (HGP) was determined by subtracting the glucose infusion rate from the total glucose appearance rate. The plasma concentration of $^{3}H_2O$ was determined by the difference between ^{3}H counts with and without drying. Whole-body glycolysis was calculated from the rate of the increase in plasma $^{3}H_2O$ concentration divided by the specific activity of plasma ^{3}H-glucose, as previously described[5]. Whole-body glycogen synthesis was estimated by subtracting whole-body glycolysis from whole-body glucose uptake, assuming that glycolysis and glycogen synthesis account for the majority of insulin-stimulated glucose uptake[6]. To determine individual tissue glucose uptake, tissue samples were homogenized, and the supernatants were subjected to an ion-exchange column to separate tissue ^{14}C-2-DG-6-phosphate (2-DG-6-P) from 2-DG. Tissue glucose uptake was calculated from the area under the curve of plasma ^{14}C-2-DG profile for the last 45 min of the clamp and muscle ^{14}C-2-DG-6-P content, as previously described[5].

***In vivo* fatty acid oxidation.** *In vivo* fatty acid oxidation rate was determined by the rate of $^{14}CO_2$ production after infusion of 3 μCi of [1-^{14}C]-oleic acid (PerkinElmer) as previously

described[7]. Briefly, 300 μg of cold oleic acid (Sigma) conjugated to fatty acid-free BSA (Sigma) was injected intraperitoneally into mice with [1-^{14}C]-oleic acid (3 μCi) at 9 AM. Mice were put in metabolic chambers connected with 1 N NaOH trap to capture expired $^{14}CO_2$. ^{14}C radioactivity from NaOH trap was counted at 30-min interval over the next 4 h, and the slope for the initial 2 h was plotted because captured radioactivity is saturated after 2 h.

***Ex vivo* fatty acid oxidation.** WAT, BAT, skeletal muscle (extensor digitorum longus) and the liver were quickly removed from mice and placed in 25-ml flasks fitted with center wells containing 1 N NaOH and a filter paper strip to trap $^{14}CO_2$. Flasks were capped with bottle stoppers. Incubation media contained 3 ml of Krebs-Ringer phosphate buffer, 2 μCi of [1-^{14}C] oleic acid and cold oleic acid (0.6 mM final concentration) in complex with BSA. Tissues were incubated in shaking water bath at 37 °C for 60 min (WAT and skeletal muscle) or 30 min (BAT and liver). After shaking incubation, 1 ml of 0.5 N sulfuric acid was injected into the media to release $^{14}CO_2$. Flasks were maintained at 50 °C for 3 h to transfer $^{14}CO_2$ to NaOH in the center well. After acid treatment, contents of the center well were transferred to scintillation fluid and ^{14}C radioactivity was counted.

***Ex vivo* lipolysis assay.** Epididymal fat pads were removed fresh from mice and finely minced with ultra-thin razor blades. Fragments of adipose tissues were gently washed once by inverting and centrifuged at 100 × g for 5 min in Krebs-Ringer bicarbonate buffer (KRBB), pH 7.4 (Sigma). The fragments (100 mg) were transferred to KRBB supplemented with 25 mM HEPES and 1% BSA. Samples were treated with vehicle (sterile water) or recombinant Fgf21 (BioVision) of the final concentrations of 0.2–1 μg ml^{-1} at 37 °C for 3 h. Glycerol released from

adipose tissues was then measured using a Glycerol Determination Kit (Sigma).

Treadmill exercise. The treadmill test was performed using the Exer-6M (Columbus Instruments). Twenty-four-week-old male mice were warmed up at a speed of 5 m per min for 10 min. Every subsequent 10 min, the speed was increased by 5 m per min. Then, mice ran until exhaustion at a maximum speed of 25 m per min. Exhaustion was defined as the inability to continue regular treadmill running despite repeated electric prodding to the mice. Running time was measured, and running distance was calculated.

Microarray analysis. Total RNA was extracted with TRIzol (Invitrogen) and purified using RNeasy columns (Qiagen) according to the manufacturer's instruction. Microarray analysis was carried out by Macrogen Inc. Briefly, biotinylated complementary RNAs were amplified and purified using an Illumina RNA amplification kit (Ambion) according to the manufacturer's instruction. Labeled cRNA samples were hybridized to each Mouse-8 Expression Bead Array according to the manufacturer's instruction (Illumina). Detection of array signal was carried out using FluoroLink streptavidin-Cy3 (GE Healthcare Bio-Sciences). Arrays were scanned with an Illumina bead array Reader confocal scanner, and the scanned images were analyzed using an Illumina BeadStudio v3.1.3 software (Gene Expression Module v3.3.8).

Plasmid constructs. pcDNA3-HA-*Atf4* and pcDNA3-HA-*p62* were constructed by inserting human *ATF4* and *p62* fragments, respectively, into EcoRI/XhoI-digested pcDNA3-HA vector. pGL3B-*PPARα* (-2150/+300) was constructed by inserting PCR fragment of human *PPARα*

promoter into KpnI/MluI-digested pGL3B vector. PPRE-luc, Gal4-tk-luc, pcDNA3/*Pparα* and pCMX/Gal4N/*Pparα* have been described[8]. Nucleotide sequence of the 5'-flanking region of *Fgf21* promoter was scanned, and two putative ATF4 binding sites (ATF4REs) were identified based on the nucleotide sequence. pGL3B-*Fgf21*(–2078/+129), pGL3B-*Fgf21*(–853/+129) (ATF4ΔRE1) and pGL3B-*Fgf21*(–107/+129) (ATF4ΔRE1/2) deletion mutant reporters were constructed by inserting respective PCR fragments amplified from C57BL/6 mouse liver genomic DNA into KpnI/BglII-digested pGL3B luciferase reporter. pGL3B-*Fgf21*(–1370/+129) vector has been described[9]. To create an ATF4mutRE1 point mutant reporter, 5'-CATCA-3' sequence (–1024 to –1020) of pGL3B-*Fgf21*(–1370/+129) vector was mutated to 5'-TCGAG-3' sequence by a DpnI-based site-directed mutagenesis method. An ATF4mutRE1/2 point mutant reporter was constructed by creating additional mutation at another 5'-CATCA-3' sequence (–136 to –132). Nucleotide sequences of all plasmids were confirmed by automatic sequencing.

Generation of adenovirus. Adenoviruses expressing HA-*Aft4*, HA-*p62* or sh*Atg7* were generated by homologous recombination between a linearized transfer vector (pAd-Track-CMV-HA-*Atf4*, Ad-Track-CMV-HA-*p62* or Ad-Track-ΔCMV-sh*Atg7*) and an adenoviral backbone vector (pAd-Easy) as described[10]. Mouse sh*Atg7* target sequences were as follows: 5'-AAGGTCGTGTCTGTCAAGTGC-3'. Adenovirus was amplified in 293AD cells and purified by CsCl density gradient centrifugation.

Cell culture. C2C12 and HEK293 cells were obtained from the American Type Culture Collection. *Atf4*-null or wild-type MEFs and $eIF2\alpha^{S/S}$ or $eIF2\alpha^{A/A}$ MEFs were generous gifts

from D. Ron and R.J. Kaufman, respectively. *Atg7*-null or wild-type MEFs have been described[11]. Tet-off *Atg5*-null MEFs[12] were gifted from N. Mizushima. Primary mouse hepatocytes were isolated from 16-week-old $Atg7^{F/F}$ and $Atg7^{\Delta hep}$ mice by portal vein cannulation and collagenase digestion. After purification of hepatocytes with Percoll (GE Healthcare Bio-Sciences), cells were plated and maintained in Medium 199 supplemented with 10% FBS. All cells were maintained at 37 °C in a humid atmosphere of 5% CO_2.

siRNA transfection and luciferase assay. *Aft4* siRNA (si*Atf4*) and *GFP* siRNA (siCON) were purchased from Bioneer Inc. (si*Aft4*, 5'-GCCUAGGUCUCUUAGAUGAdTdT-3'; siCON, 5'-GCAUCAAGGUGAACUUCAAdTdT-3'). *Atg7*-null or wild-type MEFs were cultured in 6-well plates and transfected with si*Atf4* (100 nM) or siCON (100 nM) using Lipofectamine 2000 (Invitrogen) according to the manufacturer's instruction. For luciferase assay, HEK293 or C2C12 cells were plated in 24-well culture plates and transfected with a firefly reporter vector (0.2 μg) and Renilla reporter vector (0.01 μg), together with indicated expression plasmids (0.2 μg) using JetPEI (PolyPlus) reagent according to the manufacturer's instruction. pcDNA3 empty vector was added to the transfection to make the same total amount of plasmid DNA per transfection. After 24 h of transfection, cells were lysed in a cell culture lysis buffer (Promega), and luciferase activity was measured. Firefly luciferase activity was normalized to Renilla luciferase activity. All assays were performed at least in triplicate.

RNA isolation, RT-PCR and real-time RT-PCR. Total RNA from various cells or tissues was prepared using TRIzol (Invitrogen) and purified using a RNA clean up kit (GeneAll) according to the manufacturer's instruction. cDNA was synthesized from 2 μg of total RNA using MMLV-

RT (Moloney Murine Leukaemia Virus) reverse transcriptase (Promega) and oligo(dT) primer at 42 °C for 1 h. An aliquot (1/30 vol) of cDNA was then subjected to PCR amplification using specific primers. Real-time RT-PCR was performed using SYBR Green I (Takara) in ABI Prism 7000 (Applied Biosystems). All expression values were normalized to L32 mRNA level.

Real-time RT-PCR primers used (5' to 3'):

Acaca	(F):CCAGGCCATGTTGAGACGCT	(R):ATCACAGAGCGGACGCCATC
Acacb	(F):CGTGGTAGACAGCAGCTGAG	(R):CCCAGGTGAAGCAGGAGATA
Acadl	(F):GGGAATGAAAGCTCAGGACA	(R):AGAATCCGCATTAGCTGCAT
Acadm	(F):AGGTTTCAAGATCGCAATGG	(R):CATTGTCCAAAAGCCAAACC
AdipoQ	(F):GATGTTGGAATGACAGGAG	(R):TACACCGTGATGTGGTAAGA
Asns	(F):AACGCTTGATGACAGACCGG	(R):CCTTTCTAGCGGCCAGGAGA
Atf4	(F):AGCAAAACAAGACAGCAGCC	(R):ACTCTCTTCTTCCCCCTTGC
Atg7	(F):TGTGGAGCTGATGGTCTCTG	(R):TGATGGAGCAGGGTAAGACC
Atp5o	(F):TCTGGCGCCAGTAGTCTCTT	(R):AGATGATACCCTGGGTGTTG
Cidea	(F):GCCGTGTTAAGGAATCTGCTG	(R):TGCTCTTCTGTATCGCCCAGT
Cox5b	(F):AGGCAGCTTCAGGCACCAAG	(R):GGTGGGGCACCAGCTTGTAA
Cpt1a	(F):CCGATCATGGTTAACAGCAA	(R):TGCAGCAGAGATTTGGCATA
Cpt1b	(F):CCTTATCTCCTGCAAGAATG	(R):TCGTAAGTCAGGCAGAACTT
Cycs	(F):TACCCACTCAGAAACACACA	(R):GTCTGAAGTCACGATGAGGT
Dgat2	(F):TCATGGGTGTCTGTGGGTTA	(R):CAGAGTGAAACCAGCCAACA
Dio2	(F):GGGACTCCTCTCTGTCTTTT	(R):CCAACTTCGGACTTCTTGTA

Egr1	(F):GAGAACCGTACCCAGCAGCC	(R):CGATCGCAGGACTCGACAGG
Fasn	(F):CTCCGTGGACCTTATCACTA	(R):CTGGGAGAGGTTGTAGTCAG
Fgf21	(F):TACACAGATGACGACCAAGA	(R):GGCTTCAGACTGGTACACAT
G6pc	(F):TCCTCTTTCCCATCTGGTTC	(R):TATACACCTGCTGCGCCCAT
Igfbp2	(F):AGAAGGTCAATGAACAGCAC	(R):GCACTGCTTAAGGTTGTACC
Il15	(F):GAATACATCCATCTCGTGCTA	(R):TTTGCAAAAACTCTGTGAAGG
Il6	(F):TTGCCTTCTTGGGACTGATGC	(R):GTATCTCTCTGAAGGACTCTGG
L32	(F):CAGTCAGACCGATATGTGAA	(R):TAGAGGACACATTGTGAGCA
Lipe	(F):AAGGACTTGAGCAACTCAGA	(R):TTGACTATGGGTGACGTGTA
Mgll	(F):GACGGACAGTACCTCTTTTG	(R):AGAAAAGTAGGTTGGCCTCT
Mthfd2	(F):AGCACACGATCCTTGCAGAC	(R):CACCAGGGACGGGAGTGATA
Myh1	(F):CTGGATGCTGAGATTAGGAG	(R):TGTTCATTTTCCACTTCTCC
Myh2	(F):GAAAGCTAAGAAAGCCATCA	(R):GTTTATCCACCAAATCCTGA
Myh4	(F):CTGGAACAGACAGAGAGGAG	(R):TGGTAGGTGAGTTCCTTCAC
Myh7	(F):AAGAAGAAGATGGATGCAGA	(R):AGGTTCTTCCTGTCTTCCTC
Ndufb5	(F):TCCTAGACTCGGAGTCGGAA	(R):AACTTCCTGCTCCTTTAACC
Pck1	(F):GATGGGCATATCTGTGCTGG	(R):CAGCCACCCTTCCTCCTTAG
Pnpla2	(F):CATGATGGTGCCCTATACTC	(R):GTGAGAGGTTGTTTCGTACC
Ppara	(F):GGATGTCACACAATGCAATTCG	(R):TCACAGAACGGCTTCCTCAGGT
Pparg	(F):ATCCCTGGTTTCATTAACCT	(R):GCTCCATAAAGTCACCAAAG
Ppargc1a	(F):ATACCGCAAAGAGCACGAGAA	(R):CTCAAGAGCAGCGAAAGCGTCACA
Prdm16	(F):AGCCCTCGCCCACAACTTGC	(R):TGACCCCCGGCTTCCGTTCA
Scd1	(F):TGGAAATGCCTTTGAGATGG	(R):CCAGCCAGCCTCTTGACTAT
Slc3a2	(F):GGGGAGCGTACTGAATCCCT	(R):CTGAAGGCCAAGCTCATCCC

Slc6a9	(F):GTTGGCGCTTTGTTTCTCCG	(R):TCTGCTTGGCTTTGTGGCAT
Srebf1c	(F):TGCGGCTGTTGTCTACCATA	(R):TGCTGGAGCTGACAGAGAAA
Tnf	(F):CCTGTAGCCCACGTCGTAGC	(R):TTGACCTCAGCGCTGAGTTG
Ucp1	(F):TATCATCACCTTCCCGCTG	(R):GTCATATGTTACCAGCTCTG
Ucp2	(F):CTGGCAGGTAGCACCACAG	(R):AAAGGTGCCTCCCGAGATT
Ucp3	(F):CCTCTACGACTCTGTCAAGC	(R):GACAGGGGAAGTTGTCAGTA
Uqcrb	(F):ACTTACCCAGAAGGCAGCG	(R):TGCCCACTCTTCTCTCTCCT

Antibodies. For immunoblot analysis, Santa Cruz antibodies were used: Hsp90 (sc-7947, 1:2,000 dilution), β-actin (sc-47778, 1:1,000 dilution), Atf4 (sc-200, 1:1,000 dilution), Tom20 (sc-11415, 1:1,000 dilution), Pgc1α (sc-13067, 1:1,000 dilution). Cell Signaling antibodies were used: Atg7 (#2631, 1:1,000 dilution), HA (#2367, 1:1,000 dilution), total Eif2α (#9722, 1:2,000 dilution), phospho-Eif2α Ser51 (#3597, 1:1,000 dilution), total Erk (#4695, 1:2,000 dilution), phospho-Erk Thr202/Tyr204 (#4370, 1:1,000 dilution), phospho-Frs2α Tyr196 (#3864, 1:1,000 dilution). Calbiochem antibodies were used: Ucp1 (662045, 1:1,000 dilution), Ucp2 (144157, 1:1,000 dilution). Millipore antibody was used: Ucp3 (AB3046, 1:1,000 dilution). Novus Biologicals antibody was used: Lc3 (NB100-2331, 1:1,000 dilution). R&D Systems antibody was used: Fgf21 (AF3057, 1:1,000 dilution). For immunohistochemical staining of β-cells, insulin-specific antibody (A0564, Dako, 1:100 dilution) was used. For immunofluorescent staining of muscle fibers, p62-specific (GP62-C, Progen, 1:100 dilution) and ubiquitin-specific (Z0458, Dako, 1:100 dilution) antibodies were used.

Immunoblot analysis. Cells and tissues were lysed in a radio-immunoprecipitation assay buffer

[RIPA; 50 mM Tris-HCl, pH 7.4, 150 mM NaCl, 1 mM EDTA, 1% (v/v) NP-40 (Nonidet P-40), 0.25% sodium deoxycholate, 1 mM PMSF and protease inhibitors (Roche)] for 30 min on ice, and whole lysates were obtained by subsequent centrifugation at 13,000 × g for 20 min at 4 °C. Protein concentration was determined by the Bradford assay (Bio-Rad). Lysates (50–100 μg of protein) were subjected to SDS/PAGE (8–12% gels) and transferred to PVDF membranes (Millipore). Membranes were then incubated with primary antibodies in Tris-buffered saline containing 0.05% Tween-20 (TBST) supplemented with 5% (w/v) non-fat dry milk. Bands were visualized using an enhanced chemiluminescence (ECL) system (Amersham Biosciences). Protein carbonylation was determined using an OxyBlot Protein Oxidation Detection Kit (Millipore). Relative band densities were quantified using an NIH ImageJ Software.

Purification of mitochondria and oxygen consumption. Skeletal muscle tissues were homogenized in a mitochondrial isolation buffer (pH 7.4) containinig 50 mM sucrose, 200 mM mannitol, 5 mM potassium phosphate, 1 mM EGTA, 5 mM MOPS, 0.1% BSA and protease inhibitors using a medium-fitting glass-teflon Potter-Elvehjem homogenizer. Resultant homogenate was centrifuged at 1,000 × g for 5 min at 4 °C. Supernatant was centrifuged again at 10,000 × g for 10 min at 4 °C. Mitochondrial pellets were collected and diluted in 3 volumes of mitochondrial isolation buffer. Mitochondria oxygen uptake was measured using a Clark-type oxygen electrode (Instech) in a 600 μl air-saturated chamber at room temperature. The respiration medium consisted of 145 mM KCl, 30 mM HEPES, 5 mM KH_2PO_4, 3 mM $MgCl_2$, 0.1 mM EGTA, and 0.1% BSA (pH 7.4). Mitochondrial state 4 respiration was determined using 5 mM glutamate/malate as substrates. State 3 (active) respiration was measured after adding 0.5 mM ADP to the medium. Oxygen uptake was expressed in nanomoles of O_2 per minute per

milligram of protein.

Nature Medicine doi:10.1038/nm.3014

SUPPLEMENTAL REFERENCES

1. Kubicky, R.A., Wu, S., Kharitonenkov, A. & De Luca, F. Role of fibroblast growth factor 21 (FGF21) in undernutrition-related attenuation of growth in mice. *Endocrinology* **153**, 2287-95 (2012).
2. De Sousa-Coelho, A.L., Marrero, P.F. & Haro, D. Activating transcription factor 4-dependent induction of FGF21 during amino acid deprivation. *Biochem J* **443**, 165-71 (2012).
3. Cheng, Y. et al. Leucine deprivation decreases fat mass by stimulation of lipolysis in white adipose tissue and upregulation of uncoupling protein 1 (UCP1) in brown adipose tissue. *Diabetes* **59**, 17-25 (2010)
4. Choi, C.S. et al. Continuous fat oxidation in acetyl-CoA carboxylase 2 knockout mice increases total energy expenditure, reduces fat mass, and improves insulin sensitivity. *Proc Natl Acad Sci U S A* **104**, 16480-5 (2007).
5. Youn, J.H. & Buchanan, T.A. Fasting does not impair insulin-stimulated glucose uptake but alters intracellular glucose metabolism in conscious rats. *Diabetes* **42**, 757-63 (1993).
6. Rossetti, L. & Giaccari, A. Relative contribution of glycogen synthesis and glycolysis to insulin-mediated glucose uptake. A dose-response euglycemic clamp study in normal and diabetic rats. *J Clin Invest* **85**, 1785-92 (1990).
7. Cha, S.H., Hu, Z., Chohnan, S. & Lane, M.D. Inhibition of hypothalamic fatty acid synthase triggers rapid activation of fatty acid oxidation in skeletal muscle. *Proc Natl Acad Sci U S A* **102**, 14557-62 (2005).
8. Kim, K.H. et al. Hepatitis B virus X protein induces hepatic steatosis via transcriptional activation of SREBP1 and PPARgamma. *Gastroenterology* **132**, 1955-67 (2007).

9. Wang, H., Qiang, L. & Farmer, S.R. Identification of a domain within peroxisome proliferator-activated receptor gamma regulating expression of a group of genes containing fibroblast growth factor 21 that are selectively repressed by SIRT1 in adipocytes. *Mol Cell Biol* **28**, 188-200 (2008).

10. He, T.C. et al. A simplified system for generating recombinant adenoviruses. *Proc Natl Acad Sci U S A* **95**, 2509-14 (1998).

11. Komatsu, M. et al. Impairment of starvation-induced and constitutive autophagy in Atg7-deficient mice. *J Cell Biol* **169**, 425-34 (2005).

12. Hosokawa, N., Hara, Y. & Mizushima, N. Generation of cell lines with tetracycline-regulated autophagy and a role for autophagy in controlling cell size. *FEBS Lett* **581**, 2623-9 (2007).